Two-Dimensional Spectroscopy for the Study of Ion Coulomb Crystals

A. Lemmer,[1] C. Cormick,[1] C. T. Schmiegelow,[2] F. Schmidt-Kaler,[2] and M. B. Plenio[1]
[1]*Institut für Theoretische Physik, Albert-Einstein-Allee 11, Universität Ulm, 89069 Ulm, Germany*
[2]*QUANTUM, Institut für Physik, Universität Mainz, D-55128 Mainz, Germany*
(Received 30 June 2014; published 18 February 2015)

Ion Coulomb crystals are currently establishing themselves as a highly controllable test bed for mesoscopic systems of statistical mechanics. The detailed experimental interrogation of the dynamics of these crystals, however, remains an experimental challenge. In this work, we show how to extend the concepts of multidimensional nonlinear spectroscopy to the study of the dynamics of ion Coulomb crystals. The scheme we present can be realized with state-of-the-art technology and gives direct access to the dynamics, revealing nonlinear couplings even in the presence of thermal excitations. We illustrate the advantages of our proposal showing how two-dimensional spectroscopy can be used to detect signatures of a structural phase transition of the ion crystal, as well as resonant energy exchange between modes. Furthermore, we demonstrate in these examples how different decoherence mechanisms can be identified.

DOI: 10.1103/PhysRevLett.114.073001 PACS numbers: 37.10.Ty, 05.30.-d, 05.45.-a, 63.20.K-

Two-dimensional (2D) spectroscopy was first proposed and realized in the context of nuclear magnetic resonance (NMR) experiments and has proven to be a very valuable tool in the investigation of complex spin systems [1]. By properly designed pulse sequences complicated spectra can be unraveled by the separation of interactions originating from different physical mechanisms to different frequency axes. The method allows for the estimation of spin-spin couplings in complex spin systems and the identification of different sources of noise. 2D spectroscopy has been adapted with remarkable success to other fields, facilitating the investigation of anharmonic molecular vibrational spectra in the infrared [2], electronic dynamics in molecular aggregates [3] and photosynthetic pigment-protein complexes [4], and photochemical reactions [5].

Here we propose and analyze the application of 2D spectroscopy for the precise experimental characterization of nonlinear dynamics in few- or many-body systems of interest for quantum optics, in particular, in trapped-ion Coulomb crystals. The excellent control over the internal and motional degrees of freedom makes trapped atomic ions [6] a versatile tool to study statistical mechanics of systems in and out of equilibrium [7–9]. A paradigmatic example is provided by the linear-to-zigzag structural transition [10,11]. In the vicinity of the transition, the usual harmonic treatment of the motion breaks down and nonlinear terms in the potential are essential for understanding the dynamics of the Coulomb crystal. Nonlinearities added to the trap potential have also been proposed for the implementation of the Frenkel-Kontorova model [12] and the Bose-Hubbard model [13]. The scheme we present can be used for the analysis of nonlinear dynamics, and, more generally, it represents a new approach for the interrogation of complex quantum systems constructed from ion crystals. Some features of 2D spectroscopy are especially appealing in this context: it can provide information that is not accessible in 1D Ramsey-type experiments, it can filter out the contribution from purely harmonic terms, and it allows us to distinguish dephasing and relaxation due to environmental dynamical degrees of freedom from fluctuations between subsequent experimental runs. We note that, as opposed to a related scheme [14], our proposal requires neither the technically demanding individual addressing of ions nor ground-state cooling. Furthermore, a purely harmonic evolution produces no 2D spectroscopic signal in our protocol [15]. We expect that these properties constitute key elements for the investigation of nonlinear dynamics in large crystals [23]. After a brief review of the general formalism of 2D spectroscopy we illustrate its usefulness in ion-trap experiments with two case examples.

2D spectroscopy [1–3].—After state initialization, a general multidimensional spectroscopy experiment consists of a sequence of n electromagnetic pulses on the system under investigation separated by intervals of free evolution. The action of the kth pulse on the system's density matrix is described by a superoperator $\hat{P}_k$. It is followed by a period of time t_k in which the system evolves under a Hamiltonian H_k, with an associated superoperator $\hat{H}_k$, and additional dissipative processes described by $\hat{\Gamma}_k$ resulting in a Lindblad superoperator $\hat{L}_k = -i\hat{H}_k - \hat{\Gamma}_k$. The temporal variables t_k are scanned over an interval $[0, t_k^{\max}]$ and at the end of every experiment an operator M is measured giving a signal

$$s(t_1, \ldots, t_n) = \mathrm{Tr}[M\rho(t_1, \ldots, t_n)], \quad (1)$$

$$\rho(t_1, \ldots, t_n) = \exp[\hat{L}_n t_n]\hat{P}_n \cdots \exp[\hat{L}_1 t_1]\hat{P}_1\rho_0, \quad (2)$$

where ρ_0 is the initial state and we assume for simplicity that $\hat{L}_k$ is time independent. The frequency-domain signal,

which contains spectral information of the Liouvillians governing the free evolution periods, is extracted by a Fourier transform of the signal $s(t_1, \ldots, t_n)$ in one or several time variables. A 2D spectrum displays the signal as a function of two of the time or frequency variables.

In the implementation we propose, the pulses correspond to phase-controlled displacements $\hat{P}_k\rho = D(\alpha_k)\rho D(\alpha_k)^\dagger$ on one of the motional modes of the ion crystal. Here, $D(\alpha_k) = \exp[\alpha_k a^\dagger - \alpha_k^* a]$ with $\alpha_k = |\alpha_k| e^{i\phi_k}$ and a the annihilation operator of the mode. We consider sequences involving four such pulses, followed by a measurement of the mode population. For small α_k, the displacement operators can be expanded in powers of α_k. Using this expansion and phase cycling, one can identify the coherence transfer pathways that contribute to the final signal [1,15]. This allows for an understanding of the physical origin of each spectral peak.

Nonlinear terms in the Coulomb interaction between trapped ions.— We consider N singly charged ions of mass m in a linear Paul trap described by an effective harmonic confining potential. Taking into account the mutual Coulomb repulsion between ions the Hamiltonian of the system reads

$$H = \sum_{i,\mu}\left(\frac{p_{i\mu}^2}{2m} + \frac{1}{2}m\omega_\mu^2 r_{i\mu}^2\right) + \frac{1}{2}\sum_{i\neq j}\frac{e^2}{4\pi\epsilon_0}\frac{1}{|\mathbf{r}_i - \mathbf{r}_j|}. \quad (3)$$

Here $\{\omega_\mu\}_{\mu=x,y,z}$ denote the trap frequencies, $r_{i\mu}(p_{i\mu})$ the position (momentum) of ion i in spatial direction μ, and ϵ_0 the vacuum permittivity. If $\omega_x, \omega_y \gg \omega_z$, cold ions arrange on a string along the z axis and perform small oscillations $\delta r_{i\mu}(t) = r_{i\mu}(t) - r_{i\mu}^0$ about their equilibrium positions $r_{i\mu}^0$. The Hamiltonian expanded to second order in $\delta r_{i\mu}(t)$ can be diagonalized so that the motional degrees of freedom are described by a set of $3N$ uncoupled harmonic oscillators:

$$H_0 = \hbar\omega_z\sum_n(\sqrt{\gamma_n^x}a_n^\dagger a_n + \sqrt{\gamma_n^y}b_n^\dagger b_n + \sqrt{\lambda_n^z}c_n^\dagger c_n). \quad (4)$$

Here, $a_n(b_n, c_n)$ denotes the annihilation operator for mode n in the $x(y, z)$ direction and λ_n^z and $\gamma_n^{x/y}$ are the eigenvalues of the Hessian matrices of the potential in the different spatial directions. In each direction, $n = 1$ denotes the center-of-mass mode and $n = N$ the mode where neighboring ions move in counterphase. In transverse directions this mode is dubbed the zigzag (ZZ) mode.

We consider a linear chain along z with $\omega_y > \omega_x$ and focus on dynamics involving transverse motion in the x direction. The first, nonlinear, corrections to H_0 arise with the third [24] and fourth-order terms [15] in the Taylor expansion of the Coulomb potential :

$$H^{(3)} = 3\frac{z_0}{4l_z}\hbar\omega_z\sum_{n,m,p}\frac{D_{nmp}^{(3)}}{\sqrt[4]{\gamma_n^x\gamma_m^x\lambda_p^z}}(a_n + a_n^\dagger)(a_m + a_m^\dagger)(c_p + c_p^\dagger), \quad (5)$$

$$H^{(4)} = 3\left(\frac{z_0}{4l_z}\right)^2\hbar\omega_z\sum_{n,m,p,q}D_{nmpq}^{(4)}\frac{(a_n + a_n^\dagger)(a_m + a_m^\dagger)}{\sqrt[4]{\gamma_n^x\gamma_m^x}} \times\left[\frac{(a_p + a_p^\dagger)(a_q + a_q^\dagger)}{\sqrt[4]{\gamma_p^x\gamma_q^x}} + \frac{2(b_p + b_p^\dagger)(b_q + b_q^\dagger)}{\sqrt[4]{\gamma_p^y\gamma_q^y}} - \frac{8(c_p + c_p^\dagger)(c_q + c_q^\dagger)}{\sqrt[4]{\lambda_p^z\lambda_q^z}}\right]. \quad (6)$$

Here, $z_0 = \sqrt{\hbar/(2m\omega_z)}$ is the spread of the ground-state wave function for the axial center-of-mass mode and $l_z = [e^2/(4\pi\epsilon_0 m\omega_z^2)]^{1/3}$ is the length scale of the inter-ion spacing set by the axial trapping, while $D_{nmp}^{(3)}$ and $D_{nmpq}^{(4)}$ depend on the dimensionless equilibrium positions and normal-mode coefficients. We report only terms involving modes in the x direction [15].

Under typical operating conditions $z_0/4l_z \approx 10^{-3}$ as ω_z usually lies in the MHz range. This implies that third-order contributions of the perturbation expansion represent small corrections to the harmonic Hamiltonian H_0. However, the trap frequencies can be tuned to resonances so that there is coherent energy transfer between modes [24]. In this regime, nonlinear terms cannot be neglected. We note that such resonances become generic in systems with many ions. Sufficiently far from resonances, the dominant effect of the third-order terms is given by Kerr-type shifts of the mode frequencies found in second-order perturbation theory [25]. The fourth-order contributions in the Taylor expansion of the Coulomb potential also result in such shifts. Both contributions are smaller than the harmonic terms by roughly a factor $(z_0/4l_z)^2 \approx 10^{-6}$. These small cross-Kerr nonlinearities can become important in quantum information experiments where shifts of the order of 1–20 Hz were found to affect the achieved fidelity [26]. Moreover, fourth-order contributions of the Coulomb potential are fundamental for the description of structural transitions such as the linear-to-zigzag transition [10,11].

In the following, we analyze how to access the nonlinear dynamics of the ions by means of 2D spectroscopy. To this end we consider a linear string of $N = 3$ ions, which displays the essential characteristics of nonlinear mode coupling, while the reduced complexity of the 2D spectra facilitates their interpretation. With increasing system size the linear spectrum becomes more crowded, resonances may appear without being deliberately tuned, and ground-state cooling of all modes becomes harder, thus making cross-Kerr energy shifts more problematic. As 2D spectroscopy can deal with all of these problems it becomes increasingly useful with increasing system size.

Signatures of the onset of a structural transition from 2D spectroscopy.—The linear-to-zigzag transition occurs when the confining potential in one radial direction is reduced below a critical value at which the ions break out of the linear structure. We consider a case in which the potential in

the x direction is lowered approaching, but not crossing, the linear-to-zigzag transition. On approach to the structural transition, the ZZ-mode frequency $\omega_{\mathrm{ZZ}} = \sqrt{\gamma^x_{\mathrm{ZZ}}}\omega_z$ approaches zero as γ^x_{ZZ} goes to zero. This leads to an increase of the fourth-order terms in Eq. (6) involving γ^x_{ZZ}. The increase is fastest for the term whose coefficient scales as $1/\gamma^x_{\mathrm{ZZ}}$, which contains nonrotating terms $\propto (a^\dagger_{\mathrm{ZZ}})^2 a^2_{\mathrm{ZZ}}$ and $\propto a^\dagger_{\mathrm{ZZ}} a_{\mathrm{ZZ}}$. The former corresponds to a self-interaction of the ZZ mode, while the second term shifts the ZZ mode frequency.

The effects of the third-order Hamiltonian Eq. (5) are comparable to the contributions of the fourth-order terms, but carry opposite signs so partial cancellations occur. In an interaction picture with respect to the normal modes, we obtain an effective Hamiltonian $H^{(4)}_{\mathrm{eff}} = H_s + H_d$ consisting of the self-interaction (SI) part

$$H_{\mathrm{s}} = \hbar\left(\frac{\Omega_{\mathrm{SI}}}{2}(a^\dagger_{\mathrm{ZZ}})^2 a^2_{\mathrm{ZZ}} + \Delta\omega_{\mathrm{ZZ}} a^\dagger_{\mathrm{ZZ}} a_{\mathrm{ZZ}}\right), \tag{7}$$

and a dephasing part arising from cross-Kerr couplings:

$$H_d = \hbar a^\dagger_{\mathrm{ZZ}} a_{\mathrm{ZZ}}\left(\Omega^x_{d,2} a^\dagger_2 a_2 + \sum_{n=2,3} \Omega^y_{d,n} b^\dagger_n b_n + \Omega^z_{d,n} c^\dagger_n c_n\right). \tag{8}$$

The self-interaction strength is $\Omega_{\mathrm{SI}} = 36(z_0/4l_z)^2\omega_z D^{(4)}_{3333}/\gamma^x_{\mathrm{ZZ}}$, while the dephasing rates $\Omega^\mu_{d,n}$ scale as $1/\sqrt{\gamma^x_{\mathrm{ZZ}}}$ [15].

In order to determine the self-interaction strength, we consider a sequence of four small displacements on the ZZ mode. A measurement of the ZZ-mode population completes the experimental cycle. We choose pathways carrying the phase signature $\phi_2 - \phi_3 - \phi_4$; two example coherence transfer pathways are illustrated in Fig. 1. We are interested in the dynamics during t_1 and t_3. Our signal is given by Eqs. (1)–(2) with $M = a^\dagger_{\mathrm{ZZ}} a_{\mathrm{ZZ}}$, $t_2 = t_4 = 0$, $\alpha_k = |\alpha_k| e^{i\phi_k}$ for $k = 1, 2, 3, 4$ and $\phi_1 = 0$.

The practicality of our scheme is demonstrated by the simulation of the measurement of Ω_{SI} for a realistic experimental setting using $^{40}\mathrm{Ca}^+$ ions. The motional states of the ions can be initialized close to their ground states by Doppler and sideband cooling [27] and the displacements of the modes can be implemented by state-dependent optical dipole forces [28]. Our parameters, summarized in Table I, are sufficiently far from the structural transition so that a perturbative expansion remains valid and effective cooling of the zigzag mode is still possible. We have not taken into account the effect of micromotion [29] which would lead to minor corrections of the entries of Table I without affecting the general concepts presented here. In Table I we also give the effective dephasing rates for our choice of trap frequencies. For these parameters we expect dephasing due to cross-Kerr couplings to be the dominant source of noise, so we neglect heating in our simulations.

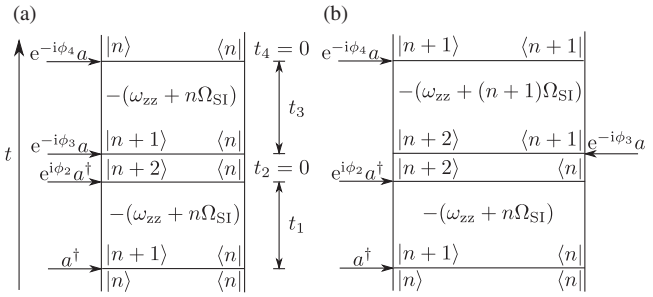

FIG. 1. Parts (a) and (b) show two example pathways carrying the phase signature $\phi_2 - \phi_3 - \phi_4$. Starting from a population all pathways have to end in a population in order to be observable. In paths (a) the coherences oscillate with the same frequency during the evolution period t_3 as during t_1 thus giving rise to diagonal peaks in the spectrum. In paths (b) the oscillation frequency during t_3 is shifted by $-\Omega_{\mathrm{SI}}$ with respect to t_1 leading to off-diagonal peaks below the main diagonal.

The main contributions to the dephasing originate from the zigzag mode in the y direction and from the Egyptian mode [15], which we include in the simulations. We make $N_{\phi_k} = 4$ phase cycles for each phase and take all $|\alpha_k| = 0.25$. We choose the initial state as a product of thermal states for the modes with mean phonon numbers of $\bar{n}_{\mathrm{ZZ}} = 1$ for the zigzag and $\bar{n} = 4$ for the other two modes. The motional Hilbert spaces are truncated including nine energy levels for the zigzag and 15 for the other two modes which includes 99% and 97% of the respective populations.

The resulting 2D spectrum presented in Fig. 2 shows two dominant lines: one along the principal diagonal, and one shifted below it. The principal diagonal is due to coherence transfer pathways where the coherences oscillate at the same frequency during t_1 and t_3. Example pathways are given in Fig. 1(a). The off-diagonal line is due to paths where the oscillation frequency during t_3 is shifted by an amount $-\Omega_{\mathrm{SI}}$ with respect to the first free evolution period t_1, exemplified in Fig. 1(b). Therefore, this line shift gives direct access to the self-interaction strength Ω_{SI}. In sharp contrast, a 1D-spectroscopy experiment with only one free evolution period would yield the information obtained by projecting the spectrum along one of the two frequency axes, so that Ω_{SI} could not be obtained (cf. Fig. 2). Note that the coherence transfer pathways in Fig. 1 would give rise to a series of separated peaks; dephasing due to thermal occupation of the other modes blurs the maxima in the diagonal direction producing the observed lines. All modes, except for the center-of-mass modes, contribute to this dephasing. Hence, by ground-state cooling of the modes contributing to dephasing one would obtain sharp and well-separated resonances in the spectrum. This, however, is experimentally very demanding for large ion crystals. Finally, we remark that phase fluctuations during the pulse sequence do not pose a problem for our protocol on the considered time scale. For the use of optical dipole forces we estimate the loss in contrast due to laser phase

TABLE I. Simulation parameters for the 2D spectrum in Fig. 2. Definitions are given in the main text.

$\omega_z/2\pi$	$\omega_x/2\pi$	$\omega_y/2\pi$	$\omega_{ZZ}/2\pi$	$t_{1/3}^{\max}$	$\Delta t_{1/3}$	$\Delta\omega_{ZZ}/2\pi$	$\Omega_{SI}/2\pi$	$\Omega_{d,3}^{y}/2\pi$	$\Omega_{d,3}^{z}/2\pi$	$\lvert\alpha_k\rvert$	N_{ϕ_k}
2 MHz	3.1012 MHz	5 MHz	131.95 kHz	2 ms	25.3 μs	15.20 kHz	5.12 kHz	0.58 kHz	−1.37 kHz	0.25	4

fluctuations to be as little as 1% for the signal of the considered coherence transfer pathways [15].

Resonant energy exchange between normal modes investigated by 2D spectroscopy.—As a further example we consider a parameter regime where the fourth-order terms are negligible and the dominant nonlinear effect in the dynamics is coherent energy exchange between two modes due to a resonance in the third-order Hamiltonian $H^{(3)}$. For a trap anisotropy $(\omega_z/\omega_x)^2 = 20/63$ we obtain a resonant coupling between the stretch mode $c_2 = c_{\mathrm{str}}$ and the zigzag mode, of the form [24]

$$H_{\mathrm{res}}^{(3)} = \hbar\Omega_{\mathrm{T}}[a_{\mathrm{ZZ}}^2 c_{\mathrm{str}}^\dagger + (a_{\mathrm{ZZ}}^\dagger)^2 c_{\mathrm{str}}]. \tag{9}$$

For the subspaces with the lowest phonon numbers, the eigenvectors and eigenvalues of $H_{\mathrm{res}}^{(3)}$ can be found analytically [15]; eigenvalues for higher occupation numbers may be found numerically. We emphasize that a Hamiltonian up to third order is an approximation valid only for low numbers of excitations, and fourth-order terms are necessary to guarantee a lower-bounded energy spectrum.

For an axial frequency $\omega_z/2\pi = 2$ MHz we obtain a coupling $\Omega_{\mathrm{T}}/2\pi = 5.9$ kHz. The nonlinear dynamics induced by $H_{\mathrm{res}}^{(3)}$ can be probed in a 2D experiment with the same pulse sequence as described before, i.e., $|\alpha_k| = 0.25$, $N_{\phi_k} = 4$ and $t_{1/3}^{\max} = 2$ ms, reducing the time increment to $\Delta t_{1/3} = 10.6$ μs. For our simulation parameters, dephasing due to other modes is negligible and the dominant source of decoherence is expected to be heating of the motional modes. Accordingly, we model the modes as damped harmonic oscillators coupled to thermal reservoirs at room temperature and assume heating rates $\dot{\bar{n}}_{\mathrm{ZZ/str}} = 0.2/0.1$ quanta ms^{-1}, a conservative estimate for macroscopic traps [27]. Furthermore, we take the initial state to be a product of thermal states with residual phonon occupation numbers $\bar{n}_{\mathrm{ZZ/str}} = 0.7/0.2$. The Hilbert spaces are truncated at six and nine excitations for the stretch and zigzag modes, respectively, thus leaving out a fraction of 10^{-4} of the populations.

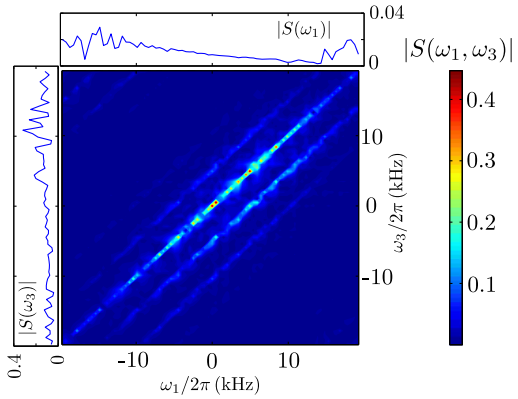

FIG. 2 (color online). The central plot shows the 2D spectrum $|S(\omega_1,\omega_3)| = |\mathcal{F}(s(t_1,t_3))|$ obtained by a four-pulse sequence with the simulation parameters given in Table I, including up to fourth-order terms in the Hamiltonian, in the neighborhood of the linear-to-zigzag transition. The diagonal peaks are due to paths of type (a) in Fig. 1. They are blurred because of static dephasing caused by thermal populations of the spectator modes leading to the diagonal line. The dominant off-diagonal [paths (b) in Fig. 1] is shifted by $-\Omega_{\mathrm{SI}}$ along the ω_3 axis and can thus be used to infer the self-interaction of the zigzag mode. The small plots along $\omega_{1/3}$ show the spectra obtained by integrating along the other frequency direction. This is the result that would be obtained by a 1D experiment with only one free evolution period $|S(\omega_{1/3})| = |S(\omega_{1/3}, t_{3/1} = 0)|$.

The resulting spectrum shown in Fig. 3 shows two bright peaks above and below the central peak, which correspond to pathways starting in the ground state. Their vertical coordinates are shifted by $\pm\sqrt{2}\Omega_T$, the eigenvalues of $H_{\mathrm{res}}^{(3)}$ for the lowest levels showing coherent energy transfer between the two modes. All peak coordinates are shifted with respect to $-\omega_{ZZ}$ by an eigenvalue of $H_{\mathrm{res}}^{(3)}$ or a linear combination thereof, from which further eigenvalues can be inferred [15]. The figure clearly shows homogeneous

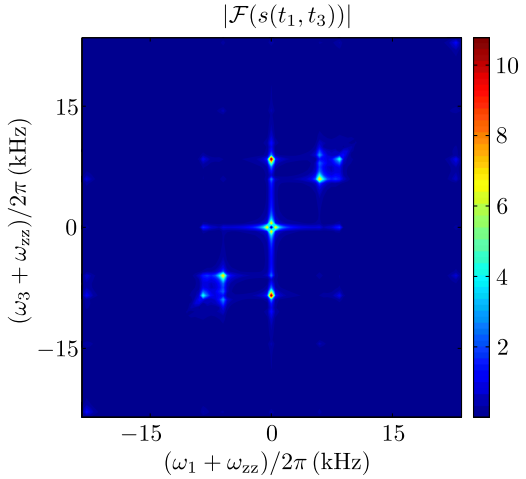

FIG. 3 (color online). 2D spectrum due to the resonant third-order terms $H_{\mathrm{res}}^{(3)}$, Eq. (9), in the Coulomb potential. Simulation parameters are given in the main text. A strong peak at $\omega_1 = \omega_3 = -\omega_{ZZ}$ was removed from the spectrum for clarity. Eigenvalues of $H_{\mathrm{res}}^{(3)}$ for low phonon numbers are identified and the effect of homogeneous broadening is clearly visible as broadening of the peaks in vertical and horizontal directions.

broadening of the peaks along the frequency axes due to the coupling to the thermal reservoirs. This illustrates how 2D spectroscopy allows for a distinction between homogeneous and inhomogeneous broadening, since the latter leads to broadening of the peaks along the diagonal as in Fig. 2.

In summary, we have shown how to extend 2D spectroscopy for the investigation of nonlinear dynamics of crystals of trapped ions. The method offers significant advantages: it does not produce any signal for purely harmonic evolution and it allows for the separation of signals which would appear superposed in a linear spectrum. It also facilitates the characterization of noise in the system: while effective static disorder gives rise to diagonal lines, dephasing and heating occurring during each experimental run manifest in broadening in the horizontal and vertical directions. Furthermore, the protocol does not require ground-state cooling, a feature which is particularly appealing for the study of large ion crystals. Note that it is well known how to achieve significant reductions in the number of measurements required to obtain 2D spectra by employing techniques from the field of matrix completion [30]. The 2D spectroscopy methods presented here form a versatile new diagnostic toolbox that may be applied well beyond the two case studies discussed here to cover all many-body models that may be realized in ion traps including spin models, structural dynamics of large ion crystals, and models in which spin and vibrational degrees of freedom are coupled.

The authors acknowledge useful discussions with U. Poschinger and M. Bruderer. This work was supported by the EU Integrating Project SIQS, the EU STREPs EQUAM and PAPETS, the Alexander von Humboldt Foundation and the ERC Synergy Grant BioQ.

[1] See R. R. Ernst, G. Bodenhausen, and A. Wokaun, *Principles of Nuclear Magnetic Resonance in One and Two Dimensions* (Oxford University Press, Oxford, 1989) and references therein.
[2] P. Hamm and M. Zanni, *Concepts and Methods of 2D Infrared Spectroscopy* (Cambridge University Press, Cambridge, England, 2011).
[3] S. Mukamel, *Principles of Nonlinear Optical Spectroscopy* (Oxford University Press, Oxford, 1995).
[4] G. S. Engel, T. R. Calhoun, E. L. Read, T.-K. Ahn, T. Mančal, Y.-C. Cheng, R. E. Blankenship, and G. R. Fleming, Nature (London) **446**, 782 (2007).
[5] S. Ruetzel, M. Diekmann, P. Nuernberger, C. Walter, B. Engels, and T. Brixner, Proc. Natl. Acad. Sci. U.S.A. **111**, 4764 (2014).
[6] D. J. Wineland, C. Monroe, W. M. Itano, D. Leibfried, B. E. King, and D. M. Meekhof, J. Res. Natl. Inst. Stand. Technol. **103**, 259 (1998).
[7] D. Porras and J. I. Cirac, Phys. Rev. Lett. **92**, 207901 (2004); A. Friedenauer, H. Schmitz, J. T. Glueckert, D. Porras, and T. Schaetz, Nat. Phys. **4**, 757 (2008); R. Islam *et al.*, Nat. Commun. **2**, 377 (2011); A. Bermudez and M. B. Plenio, Phys. Rev. Lett. **109**, 010501 (2012); P. A. Ivanov, D. Porras, S. S. Ivanov, and F. Schmidt-Kaler, J. Phys. B **46**, 104003 (2013).
[8] A. del Campo, G. DeChiara, G. Morigi, M. B. Plenio, and A. Retzker, Phys. Rev. Lett. **105**, 075701 (2010); S. Ulm *et al.*, Nat. Commun. **4**, 2290 (2013); K. Pyka *et al.*, Nat. Commun. **4**, 2291 (2013).
[9] A. Bermudez, M. Bruderer, and M. B. Plenio, Phys. Rev. Lett. **111**, 040601 (2013).
[10] A. Retzker, R. C. Thompson, D. M. Segal, and M. B. Plenio, Phys. Rev. Lett. **101**, 260504 (2008); S. Fishman, G. DeChiara, T. Calarco, and G. Morigi, Phys. Rev. B **77**, 064111 (2008).
[11] E. Shimshoni, G. Morigi, and S. Fishman, Phys. Rev. Lett. **106**, 010401 (2011); E. Shimshoni, G. Morigi, and S. Fishman, Phys. Rev. A **83**, 032308 (2011).
[12] I. Garcia-Mata, O. V. Zhirov, and D. L. Shepelyansky, Eur. Phys. J. D **41**, 325 (2007); A. Benassi, A. Vanossi, and E. Tosatti, Nat. Commun. **2**, 236 (2011).
[13] D. Porras and J. I. Cirac, Phys. Rev. Lett. **93**, 263602 (2004).
[14] M. Gessner, F. Schlawin, H. Häffner, S. Mukamel, and A. Buchleitner, New J. Phys. **16**, 092001 (2014).
[15] See Supplemental Material at http://link.aps.org/supplemental/10.1103/PhysRevLett.114.073001, which includes Refs. [16–22], for details and derivations.
[16] D. F. V. James, Appl. Phys. B **66**, 181 (1998).
[17] H. Goldstein, *Klassische Mechanik* (Akademische Verlagsgesellschaft, Frankfurt am Main, 1972).
[18] D. G. Enzer *et al.*, Phys. Rev. Lett. **85**, 2466 (2000).
[19] H. Katori, S. Schlipf, and H. Walther, Phys. Rev. Lett. **79**, 2221 (1997).
[20] A. Walther, U. Poschinger, K. Singer, and F. Schmidt-Kaler, Appl. Phys. B **107**, 1061 (2012).
[21] D. T. Gillespie, Am. J. Phys. **64**, 225 (1996).
[22] H.-P. Breuer and F. Petruccione, *The Theory of Open Quantum Systems* (Oxford University Press, Oxford, 2002).
[23] A. Dantan, J. P. Marler, M. Albert, D. Guenot, and M. Drewsen, Phys. Rev. Lett. **105**, 103001 (2010); B. C. Sawyer, J. W. Britton, A. C. Keith, C.-C. Joseph Wang, J. K. Freericks, H. Uys, M. J. Biercuk, and J. J. Bollinger, Phys. Rev. Lett. **108**, 213003 (2012).
[24] C. Marquet, F. Schmidt-Kaler, and D. F. V. James, Appl. Phys. B **76**, 199 (2003).
[25] X. R. Nie, C. F. Roos, and D. F. V. James, Phys. Lett. A **373**, 422 (2009).
[26] C. Roos, T. Monz, K. Kim, M. Riebe, H. Häffner, D. James, and R. Blatt, Phys. Rev. A **77**, 040302(R) (2008).
[27] B. King, C. Wood, C. Myatt, Q. Turchette, D. Leibfried, W. Itano, C. Monroe, and D. Wineland, Phys. Rev. Lett. **81**, 1525 (1998); H. Rohde, S. T. Gulde, C. F. Roos, P. A. Barton, D. Leibfried, J. Eschner, F. Schmidt-Kaler, and R. Blatt, J. Opt. B **3**, S34 (2001).
[28] C. Monroe, D. M. Meekhof, B. E. King, and D. J. Wineland, Science **272**, 1131 (1996).
[29] H. Landa, M. Drewsen, B. Reznik, and A. Retzker, New J. Phys. **14**, 093023 (2012).
[30] J. Almeida, J. Prior, and M. B. Plenio, J. Phys. Chem. Lett. **3**, 2692 (2012); M. Kost, J. Cai, and M. B. Plenio, arXiv:1407.6262.